On the Tropospheric Response to Anomalous Stratospheric Wave Drag and Radiative Heating

DAVID W. J. THOMPSON AND JASON C. FURTADO

Department of Atmospheric Science, Colorado State University, Fort Collins, Colorado

THEODORE G. SHEPHERD

Department of Physics, University of Toronto, Toronto, Ontario, Canada

(Manuscript received 8 June 2005, in final form 22 February 2006)

ABSTRACT

Observational and numerical evidence suggest that variability in the extratropical stratospheric circulation has a demonstrable impact on tropospheric variability on intraseasonal time scales. In this study, it is demonstrated that the amplitude of the observed tropospheric response to vacillations in the stratospheric flow is quantitatively similar to the zonal-mean balanced response to the anomalous wave forcing at stratospheric levels. It is further demonstrated that the persistence of the tropospheric response is consistent with the impact of anomalous diabatic heating in the polar stratosphere as stratospheric temperatures relax to climatology.

The results contradict previous studies that suggest that variations in stratospheric wave drag are too weak to account for the attendant changes in the tropospheric flow. However, the results also reveal that stratospheric processes alone cannot account for the observed meridional redistribution of momentum within the troposphere.

1. Introduction

A number of studies have presented observational evidence suggesting that variability in the stratospheric polar vortex has a substantial impact on the circulation of the troposphere. Cheng (1993), Baldwin et al. (1994), Perlwitz and Graf (1995), and Kitoh et al. (1996) all revealed that month-to-month variations in the Northern Hemisphere stratospheric polar vortex are coupled with a distinct wavelike pattern of anomalies in the tropospheric circulation centered over the North Atlantic sector. Thompson and Wallace (1998, 2000) subsequently argued the dynamical coupling between the stratosphere and troposphere is manifest not as a wavelike pattern in the tropospheric circulation, but as vertically coherent variations in the annular modes of extratropical variability, which are characterized by deep, zonally symmetric fluctuations in atmospheric pressure between the polar regions and the middle latitudes. Baldwin and Dunkerton (1999) demonstrated that the deep vertical coupling associated with the Northern Hemisphere annular mode (NAM) does not occur synchronously, but rather that changes in the NAM at stratospheric levels tend to precede same-signed changes in the NAM at tropospheric levels by ~10 days. Baldwin and Dunkerton (2001) later showed the associated changes in the tropospheric circulation persist as long as the corresponding changes in the lowermost stratosphere, up to ~60 days.

Several studies have noted similar behavior in numerical models. Boville (1984), Polvani and Kushner (2002), and Taguchi (2003) all found substantial changes in the tropospheric circulation reminiscent of the NAM in numerical simulations run with varying representations of the stratospheric zonal flow. Norton (2003) revealed the persistence of the tropospheric NAM is notably increased in simulations run with a well-resolved stratosphere. Recent studies have emphasized the linkages between stratospheric forcing and

Corresponding author address: David W. J. Thompson, Dept. of Atmospheric Science, Colorado State University, Fort Collins, CO 80523.
E-mail: davet@atmos.colostate.edu

© 2006 American Meteorological Society

changes in tropospheric eddy activity (e.g., Song and Robinson 2004; Kushner and Polvani 2004; Reichler et al. 2005).

Despite the apparent robustness of the aforementioned results, the principal mechanisms whereby stratospheric variability influences the tropospheric circulation remain unclear. A complete theory that explains such an influence must address two questions. First, to what extent do variations in the stratospheric zonal flow determine the amplitude and location of stratospheric wave drag? Second, how are variations in the amplitude and location of stratospheric wave drag communicated to tropospheric levels? The latter question is the focus of this study.

The simplest mechanism by which variations in stratospheric wave drag may be communicated to tropospheric levels is via geostrophic and hydrostatic adjustment to the anomalous stratospheric forcing (Eliassen 1951; Haynes et al. 1991). This so-called balanced response to stratospheric forcing is implicitly included in calculations of the remote response to stratospheric potential vorticity anomalies (Hartley et al. 1998; Ambaum and Hoskins 2002; Black 2002). Alternative mechanisms include amplification due to internal tropospheric dynamics (Song and Robinson 2004), the impact of anomalous shear at the tropopause level on vertically propagating planetary waves (Chen and Robinson 1992; Shindell et al. 1999), feedbacks between the shear at the tropopause level and the momentum flux by baroclinic eddies (Kushner and Polvani 2004), and the reflection of planetary waves (e.g., Perlwitz and Harnik 2003).

The balanced response to stratospheric forcing is generally viewed incapable of driving the entire tropospheric response because a relatively small fraction of the mass of the atmosphere resides above the tropopause. For example, Song and Robinson (2004) note that regressions based on time series of the NAM yield stratospheric wave drag anomalies of ~ 1 m s^{-1} day^{-1} and surface wind anomalies of ~ 5 m s^{-1}, whereas they calculate the balanced surface wind response to ~ 1 m s^{-1} day^{-1} of stratospheric wave drag is only ~ 0.5 m s^{-1}. However, the results cited in Song and Robinson (2004) are derived from regressions and composites based on the leading principal component of the sea level pressure field, and thus have amplitudes that correspond to a typical fluctuation in the tropospheric component of the NAM. As noted below and in section 4, the amplitude of the tropospheric response to a given change in stratospheric wave drag corresponds instead to regressions based on the stratospheric component of the NAM. In this case, changes in stratospheric wave drag of ~ 1 m s^{-1} day^{-1} are associated with zonal wind anomalies of only ~ 0.4 m s^{-1} at the surface.

The purpose of the current study is to quantify the balanced tropospheric response to observed variations in stratospheric wave drag and the associated radiative heating. In contrast to previous studies, we demonstrate that the observed tropospheric response is quantitatively consistent with geostrophic and hydrostatic adjustment to the anomalous wave drag at stratospheric levels. Hence, tropospheric feedbacks are not required to explain the amplitude of the observed tropospheric anomalies. We further show that anomalous radiative heating in the polar stratosphere contributes to the persistence of the tropospheric anomalies following the cessation of anomalous wave drag at stratospheric levels. The role of anomalous stratospheric radiative heating in maintaining the tropospheric response has apparently not been examined in previous studies.

The paper is outlined as follows. Section 2 provides a cursory review of the relevant observations. In section 3, we use a simple linear model of the zonal-mean extratropical circulation to quantify the balanced response to both the observed wave drag and associated radiative heating at stratospheric levels. In section 4, we discuss the implications of the results for dynamical coupling between the stratosphere and troposphere, and clarify what conclusions can and cannot be drawn from our analyses. Section 5 offers concluding remarks.

2. Observational analyses

The observational analyses in this study are based on daily values of the European Centre for Medium-Range Weather Forecasts (ECMWF) 40-yr reanalysis (ERA-40) (Simmons and Gibson 2000). Anomalies are formed by removing the long-term mean seasonal cycle from the data at all grid points. At all levels, the structure of the NAM is defined as the leading empirical orthogonal function (EOF) of monthly mean geopotential height anomalies over 20°–90°N during the Northern Hemisphere winter season (November–April), and daily values of the NAM index time series are found by projecting daily mean geopotential height anomalies onto the respective EOF structure function. By convention, positive (negative) values in the NAM index time series correspond to lower (higher) than normal geopotential heights over the polar cap.

The patterns of atmospheric anomalies associated with variability in the strength of the stratospheric polar vortex are found by regressing anomaly data onto standardized and inverted January–March (JFM) values of the NAM index time series at 10 hPa (hereafter referred to as NAM_{10}). The regressions are based on in-

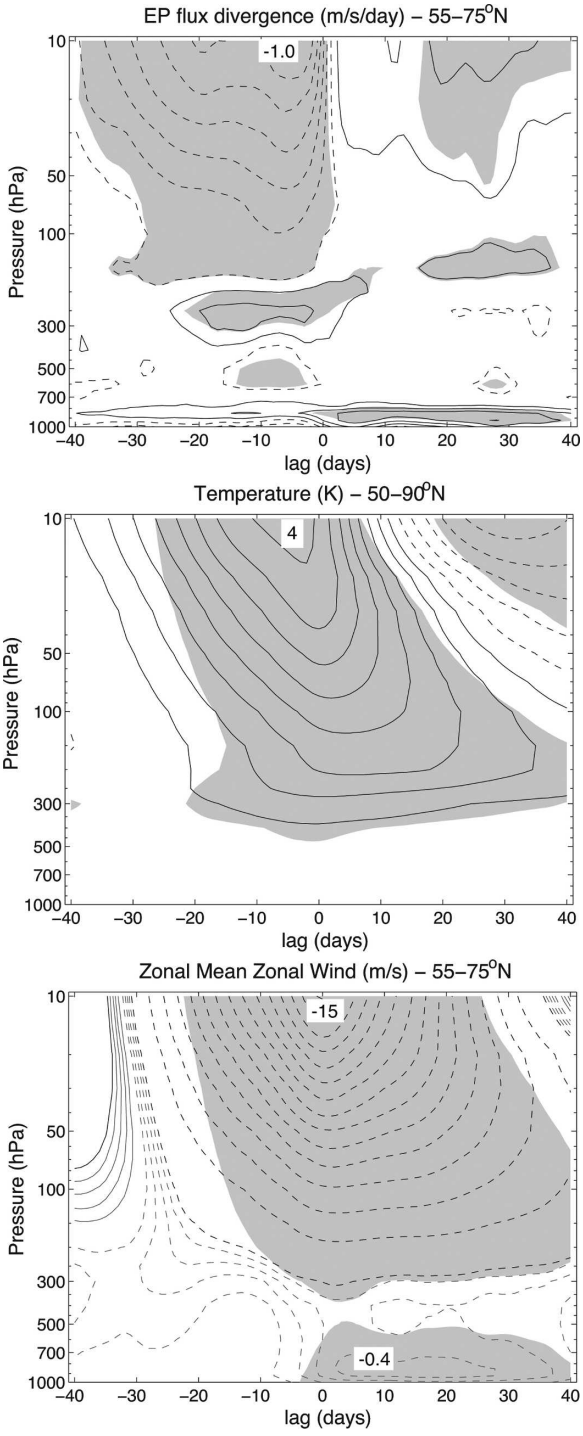

FIG. 1. Regressions onto standardized and inverted JFM values of the NAM index time series at 10 hPa (NAM_{10}) for (top) EP flux divergence anomalies averaged over 55°–75°N; (middle) temperature anomalies averaged over 50°–90°N; and (bottom) zonal-mean zonal wind anomalies averaged over 55°–75°N. The EP flux divergences are divided by $\rho_0 a \cos(\phi)$ and are in units of m s^{-1} day^{-1}. Contour intervals are (top) 0.15 m s^{-1} day^{-1} (-0.075, 0.075, 0.225, . . .); (middle) 0.5 K (-0.25, 0.25, 0.75, . . .); and (bottom) 1.0 m s^{-1} for black contours (-0.5, 0.5, 1.5, . . .); 0.1 m s^{-1} for gray contours (shown at 0.1, 0.2, 0.3, . . . for absolute values less than 0.5). Solid contours denote positive values, dashed contours negative values. Positive lags indicate NAM_{10} leads. Shading denotes regression coefficients that exceed the 95% confidence level. Numbers denote local maxima or minima.

verted values of NAM_{10} so that positive regression values correspond to higher than normal geopotential heights over the polar cap and hence weakenings of the stratospheric circumpolar zonal flow. Lag regressions are based on anomaly data extending earlier or later in the winter season as needed. For example, the regression coefficients for the zonal flow leading NAM_{10} by 10 days are found by regressing zonal wind anomalies between 22 December and 21 March onto JFM values of the NAM_{10} index time series. Statistical significance is assessed using the *t* statistic and effective sample sizes are estimated using (31) from Bretherton et al. (1999). The divergence of the Eliassen–Palm (EP) flux is defined in a manner analogous to (3.1a, b) and (3.2) in Edmon et al. (1980) and is presented in units of m s^{-1} day^{-1}.

Figure 1 shows EP flux divergence anomalies averaged 55°–75°N (top, contours), temperature anomalies averaged 50°–90°N (middle, contours), and zonal-mean zonal wind anomalies averaged 55°–75°N (bottom, contours) regressed onto standardized and inverted JFM values of the NAM_{10} index time series as a function of pressure level and lag. The gray shading in Fig. 1 corresponds to regions where the associated correlation coefficients exceed the 95% confidence level. Note the contour intervals for the zonal-mean zonal wind are different at tropospheric and stratospheric levels.

The results in Fig. 1 highlight the following key aspects of stratosphere/troposphere coupling investigated in this study:

1) In the stratosphere, the growth of circumpolar wind anomalies (Fig. 1, bottom) and polar temperature anomalies (Fig. 1, middle) coincides with periods of anomalous EP flux convergence (Fig. 1, top). In the middle stratosphere near 30 hPa, the anomalous EP flux convergence for a negative NAM_{10} anomaly peaks at $\sim$1.0 m s^{-1} day^{-1} near day -5, while the zonal-mean zonal wind and temperature anomalies peak at about -10 m s^{-1} and 5 K, respectively, shortly after day 0. The stratospheric zonal-mean zonal wind and temperature anomalies descend with time throughout the period of anomalous wave forcing.
2) Starting shortly after day 0, the stratospheric circumpolar wind and polar temperature anomalies de-

cay slowly over a period of several weeks (Fig. 1, middle and bottom). The most persistent zonal-mean zonal wind and temperature anomalies are found in the lowermost stratosphere.

3) In the troposphere, the circumpolar flow exhibits no notable changes prior to day −10, but is marked by increasing wind anomalies between days −10 and 0 that peak for a negative NAM_{10} anomaly near −0.4 m s^{-1} (Fig. 1, bottom).
4) As is the case in the lower stratosphere, the tropospheric wind anomalies decay slowly over a period of several weeks following the cessation of anomalous wave forcing at stratospheric levels. The tropospheric wind anomalies exhibit persistence substantially longer than that predicted by the ~10 day *e*-folding time scale of tropospheric variability (e.g., Feldstein 2000).

Based on the above descriptions, the observed evolution of the tropospheric and stratospheric circulation during periods of anomalous stratospheric wave drag can be decomposed into the three following stages:

The preconditioning stage (between days −30 and −15). At this time, there is substantial wave driving and increasing zonal-mean zonal wind and temperature anomalies at stratospheric levels (Fig. 1, top, middle) but minimal changes in the tropospheric zonal-mean zonal flow (Fig. 1, bottom). The absence of a tropospheric response is also evidenced in the meridional profile of the zonal wind tendencies averaged over lags −30 to −15 (Fig. 2, top left).

The growth stage (between days −10 and 0). The forcing and growth of anomalies in the stratospheric flow is accompanied by the growth of similarly signed anomalies in the tropospheric circulation (Fig. 1, bottom). For a negative NAM_{10} anomaly, the tendencies in the zonal-mean zonal flow averaged between days −10 and 0 exceed −0.5 m s^{-1} day^{-1} at 10 hPa and are roughly −0.03 to −0.04 m s^{-1} day^{-1} at tropospheric levels (Fig. 2, middle left).

The maintenance stage (between days +5 and +30). The tropospheric circulation anomalies exhibit persistence comparable to that observed in the lowermost stratosphere (Fig. 1, bottom). Averaged over days +5 to +30 of a negative NAM_{10} anomaly, the tendencies in the zonal-mean zonal flow are roughly 0.4 m s^{-1} day^{-1} westerly at 10 hPa but are negligible at tropospheric levels (Fig. 2, bottom left).

In the following section, we compare the amplitude and persistence of the tropospheric zonal wind anomalies revealed in Fig. 1 and the left panels of Fig. 2 with the balanced response to the attendant changes in wave drag and radiative heating at stratospheric levels.

3. The balanced response to anomalous stratospheric wave drag and radiative heating

a. Model description and analysis design

The balanced response to the observed anomalous stratospheric wave drag and radiative heating is estimated from the zonally symmetric, quasigeostrophic form of the governing equations linearized about a state of rest and driven by thermal and mechanical forcing (e.g., Andrews et al. 1987):

$$\frac{\partial \overline{u}}{\partial t} - f\overline{v}^* = \overline{G} + \overline{F}, \tag{1}$$

$$f\overline{u} = -a^{-1}\frac{\partial \overline{\Phi}}{\partial \phi}, \tag{2}$$

$$\frac{\partial \overline{\Phi}}{\partial p} = -\frac{R\overline{T}}{p}, \tag{3}$$

$$\frac{\partial \overline{T}}{\partial t} - \Gamma\overline{\omega}^* = \overline{Q}, \tag{4}$$

$$(a\cos\phi)^{-1}\frac{\partial}{\partial \phi}(\overline{v}^*\cos\phi) + \frac{\partial \overline{\omega}^*}{\partial p} = 0, \tag{5}$$

where $\overline{G}$, $\overline{F}$, and $\overline{Q}$ represent anomalous zonal-mean wave drag, friction and radiative heating, respectively; $\overline{v}^*$ and $\overline{\omega}^*$ the meridional and vertical components of the zonal-mean flow, respectively, in the transformed Eulerian mean (TEM) formulation; $\overline{u}$ the zonal-mean zonal flow; $\overline{\Phi}$, p, and $\overline{T}$ the zonal-mean geopotential, pressure, and temperature, respectively; f the Coriolis parameter; a the radius of Earth; ϕ latitude; R the ideal gas constant; and $\Gamma = -T_0(\partial \ln\overline{\theta}/\partial p)$ the static stability.

The lapse rate is similar to that of the 1976 United States Standard Atmosphere (COESA 1976) and is defined as

$$\gamma(p) = 3.25\left[1 + \tanh\left(\frac{p - 250}{25}\right)\right]. \tag{6}$$

The resulting lapse rate is ~6.5 K km^{-1} from 1000–250 hPa, isothermal above 200 hPa, and includes a transition layer between 200 and 250 hPa. The boundary conditions are identical to those used in Haynes and Shepherd (1989): $\overline{\omega}^* = 0$ at $p = 0$, $(\partial\overline{\Phi}/\partial t) + \overline{\omega}^*(\partial\Phi_0/\partial p) = 0$ at $p = p_0$ where $p_0 = 1000$ hPa, and $\overline{v}^* = 0$ at $\phi = \pm 90°$. While the lower boundary condition at $p = p_0$ generally applies to $\overline{\omega}$ rather than $\overline{\omega}^*$, here we consider stratospheric wave forcing only in which case $\overline{\omega} = \overline{\omega}^*$ at $p = p_0$.

The stratospheric wave drag is defined from the observations as

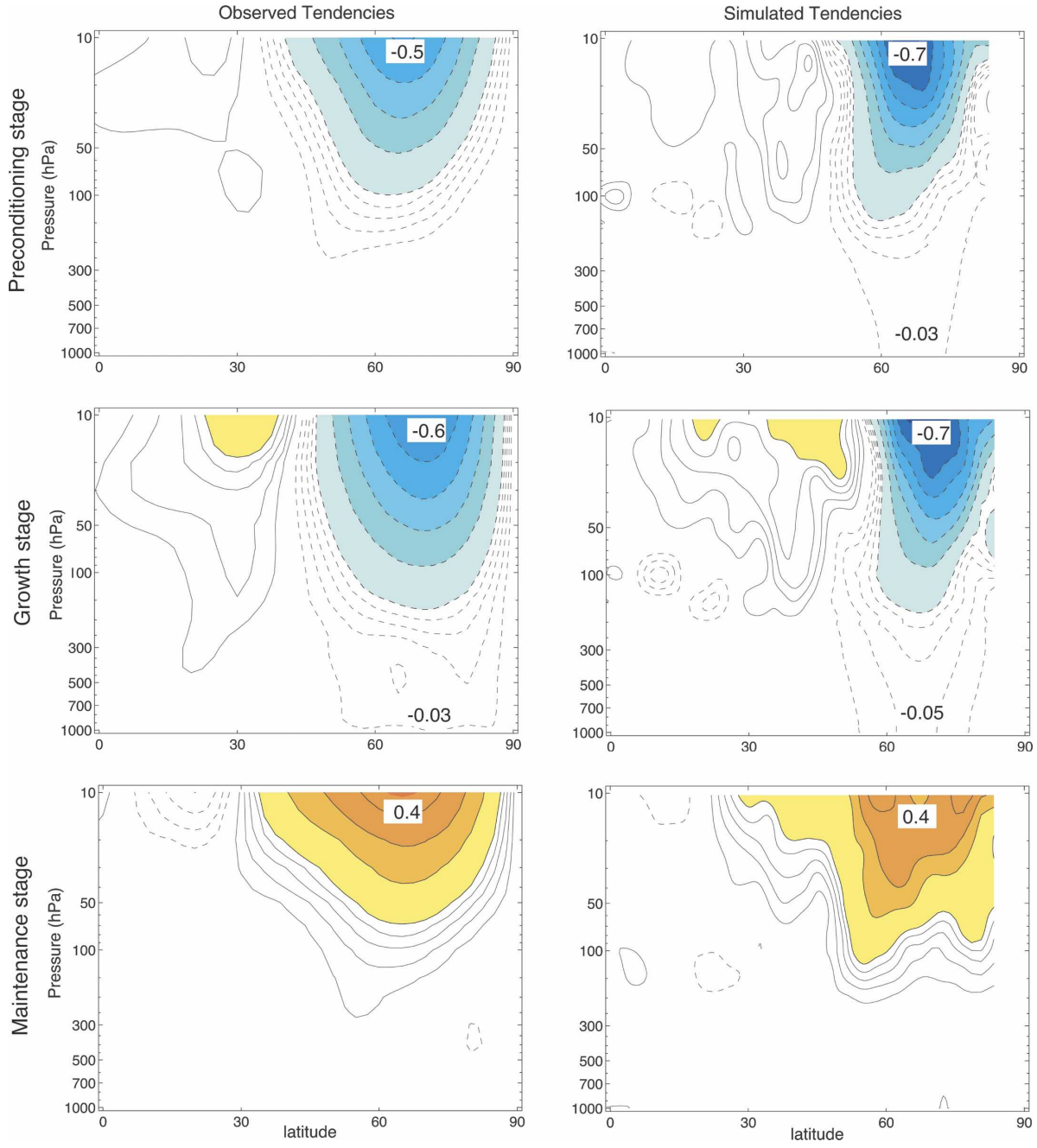

FIG. 2. (left) Zonal-mean zonal wind tendencies regressed onto standardized and inverted JFM values of the NAM_{10} index time series and averaged over the stages indicated. (right) As in (left), but for the combined simulated response to stratospheric wave driving, stratospheric radiative heating, and friction, averaged over the same stages. Contour intervals are 0.05 m s^{-1} day^{-1} for black contours (0.1, 0.15, 0.2, . . .) and 0.02 m s^{-1} for gray contours (shown at 0.02, 0.04, 0.06, . . . for absolute values less than 0.1). The zero contour is omitted. Shading denotes absolute values greater than 0.1 m s^{-1} day^{-1}. Numbers denote local maxima and minima.

$$\overline{G}(\phi, p) = \begin{cases} (\rho_0 a \cos\phi)^{-1} \nabla \cdot \mathbf{F} & 0 < p \le 100 \text{ hPa} \\ (\rho_0 a \cos\phi)^{-1} \nabla \cdot \mathbf{F} \times \tan\left[\dfrac{\pi}{4}\left(\dfrac{200 - p}{100}\right)\right] & 100 \text{ hPa} \le p \le 200 \text{ hPa} \\ 0 & p \ge 200 \text{ hPa}, \end{cases} \tag{7}$$

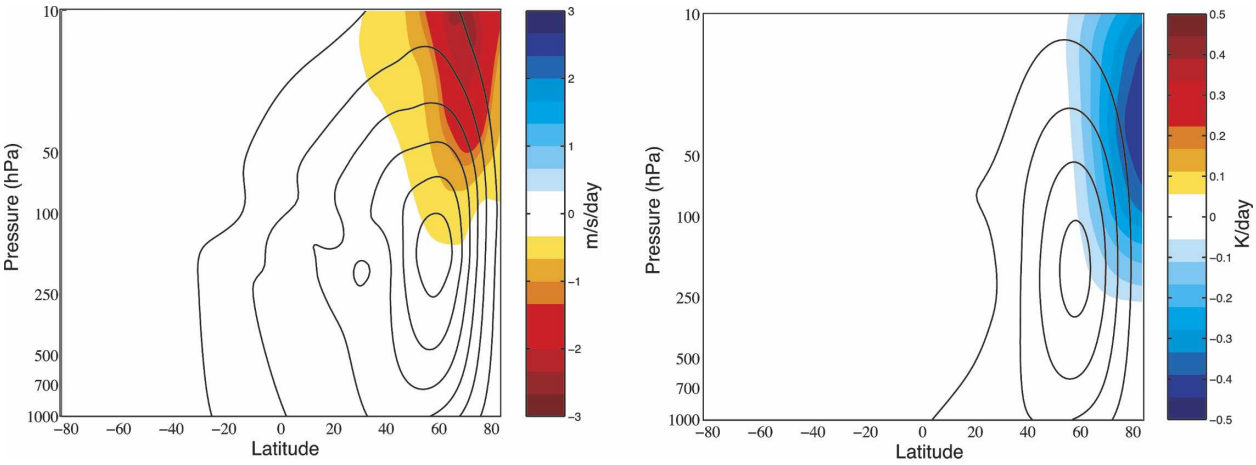

FIG. 3. (left) The model streamfunction response (contours) to the observed day −5 momentum forcing (shading). (right) As in (left), but for the model streamfunction response to the day +5 radiative heating (shading). Contour interval is 40 (left) and 20 Pa m s^{-1} (right). Units of shading are m s^{-1} day^{-1} (left) and K day^{-1} (right). Positive values of the streamfunction denote clockwise motion.

where $\nabla \cdot \mathbf{F}$ corresponds to the time history of the observed EP flux divergence anomalies regressed on inverted JFM values of the NAM_{10} index time series. Note that as in the previous section, all results are shown for the response to the anomalous forcing associated with a negative NAM_{10} anomaly.

The anomalous stratospheric radiative heating is parameterized as Newtonian cooling acting on the observed temperature anomalies and is defined as

$$\overline{Q}(\phi, p) = \begin{cases} -\alpha\overline{T} & 0 < p \le 250 \text{ hPa} \\ -\alpha\overline{T} \times \tan\left[\dfrac{\pi}{4}\left(\dfrac{350 - p}{100}\right)\right] & 250 \text{ hPa} \le p \le 350 \text{ hPa}, \\ 0 & p \ge 350 \text{ hPa} \end{cases} \tag{8}$$

where $\overline{T}$ corresponds to the time history of the observed temperatures anomalies regressed on inverted JFM values of the NAM_{10} index time series, and α = 1/(40 days) for levels below 250 hPa, increases linearly from 1/(40 days) to 1/(20 days) between 250 hPa and 95 hPa, and is 1/(20 days) for levels above 95 hPa (a similar profile of α is used in Reichler et al. 2005).

Frictional dissipation in the planetary boundary layer is parameterized as Rayleigh friction acting on the observed surface wind anomalies and is defined as

$$\overline{F}(p) = -k_s \overline{u}_{\text{sfc}} \exp\left(\frac{p - p_0}{50}\right), \tag{9}$$

where $\overline{u}_{\text{sfc}}$ is the time history of the observed 1000-hPa wind anomalies regressed on inverted JFM values of the NAM_{10} index time series and k_s = 1 day^{-1}. Note that the anomalous stratospheric radiative heating and surface friction are estimated from the observed temperature and zonal wind anomalies shown in the previous section, and thus may not be entirely due to the anomalous stratospheric wave drag. Additionally, note that since the model is linear and the temperature and wind anomalies are specified, the response to the radiative and frictional forcings depends linearly on the relaxation rates.

b. Results

Figure 3 shows sample latitude–height profiles of $\overline{G}$ (left, shading) and $\overline{Q}$ (right, shading) for periods when the stratospheric wave driving and radiative heating anomalies are substantial, superposed on the corresponding simulated changes in the mean meridional streamfunction (both panels, contours). Following Eliassen (1951), Dickinson (1968), and Haynes et al. (1991), anomalous easterly wave driving at stratospheric levels in the Northern Hemisphere gives rise to poleward flow across and equatorward flow below the axis of the forcing (left). The Coriolis force acting on the anomalous meridional flow damps the wave-driven easterly acceleration of the zonal flow at stratospheric

levels but drives an easterly acceleration of the zonal flow at tropospheric levels. Thus, anomalous easterly wave driving at stratospheric levels is associated with easterly acceleration not only at the level of the wave forcing but throughout the depth of the extratropical atmosphere.

The atmospheric response to negative anomalous radiative heating in the Northern Hemisphere polar stratosphere (i.e., as stratospheric temperatures relax to climatology) gives rise to mean meridional circulation anomalies in the same sense as the response to easterly wave drag (Fig. 3, right). However, in this case the Coriolis force acting on the induced meridional flow is not opposed by wave driving at any level. Hence, the simulated response to negative anomalous stratospheric radiative heating is marked by a westerly acceleration of the zonal flow at stratospheric levels but easterly acceleration at tropospheric levels.

The simulated responses of the tendencies in the zonal-mean zonal wind averaged 55°–75°N ($\overline{U}_{55-75N}$, where the square brackets represent the zonal mean) to observed values of $\overline{G}$, $\overline{F}$, and $\overline{Q}$ during the preconditioning (days −30 to −15), growth (days −10 to 0) and maintenance (days +5 to +30) stages are summarized in Figs. 4–6, respectively. Results are shown for the region extending from 1000–10 hPa (top panels) and highlighted at tropospheric levels between 250–1000 hPa (bottom panels). The left panels show the separate responses of $\overline{U}_{55-75N}$ to $\overline{G}$ (red), $\overline{F}$ (green), and $\overline{Q}$ (blue); the right panels show the combined responses (red) juxtaposed with the observed tendencies (black). The right panels in Fig. 2 show latitude–height profiles of the combined responses for all levels and latitudes in the Northern Hemisphere. Note that since the analysis is linear, the response to all three forcings is equal to the sum of the responses to the individual forcings.

During the preconditioning stage, the anomalous EP flux convergence at stratospheric levels gives rise to an easterly acceleration in $\overline{U}_{55-75N}$ of ~0.25 m s^{-1} day^{-1} at 50 hPa (Fig. 4, top left) and ~0.02 m s^{-1} day^{-1} at the surface (Fig. 4, bottom left). The anomalous stratospheric heating drives weak westerly acceleration in the stratosphere (Fig. 4, top left) and little change in the zonal flow at tropospheric levels (Fig. 4, bottom left). Boundary layer friction is associated with weak tendencies at all levels (Fig. 4, left).

The corresponding sums of the simulated tendencies are shown in the right panels of Fig. 4 and the top right panel of Fig. 2. The amplitudes and vertical profile of the simulated tendencies are comparable to the observations at stratospheric levels. However, at tropospheric levels the balanced response to stratospheric forcing predicts an easterly acceleration of ~0.02 m s^{-1} day^{-1} whereas the associated observed tendencies are negligible (Fig. 2, top panels; Fig. 4, bottom right).

During the growth stage, the anomalous stratospheric EP flux convergence continues to drive easterly acceleration at all levels, with simulated tendencies of about −0.3 and −0.03 m s^{-1} day^{-1} found near 50 hPa and the surface, respectively (Fig. 5, left panels). The anomalous radiative heating in the polar stratosphere gives rise to a westerly acceleration of about 0.15 m s^{-1} day^{-1} near ~50 hPa (Fig. 5, top left) but an easterly acceleration of about 0.01 m s^{-1} day^{-1} at tropospheric levels (Fig. 5, bottom left). Hence, the anomalous heating in the polar stratosphere acts to damp the response to stratospheric wave drag in the stratosphere but amplify the response to stratospheric wave drag in the troposphere. Boundary layer friction is associated with westerly acceleration anomalies of ~0.01 m s^{-1} day^{-1} in the free troposphere.

As is the case with the preconditioning stage, the sums of the simulated growth stage tendencies bear a close resemblance to the observations at stratospheric levels (Fig. 5, top right; Fig. 2, middle panels). In contrast to the preconditioning stage, the simulated growth stage tendencies also bear a resemblance to (and also, in fact, exceed) the observed tendencies at tropospheric levels (Fig. 5, bottom right). For example, at 925 hPa the combined simulated response is about −0.04 m s^{-1} day^{-1} while the observed response is roughly −0.03 m s^{-1} day^{-1} (Fig. 5, bottom right; Fig. 2, middle panels). Note that while the amplitudes of the observed and simulated tendencies are remarkably similar during the growth stage, the meridional profile of observed easterly tendencies spans a narrower range of latitudes, particularly at tropospheric levels (Fig. 2, middle panels).

During the maintenance stage, the stratosphere continues to be disturbed by anomalous radiative heating, but in this case the wave drag is westerly and comparatively weak (Fig. 6, top left). The anomalous westerly stratospheric wave drag gives rise to a westerly acceleration of the zonal flow at all levels (Fig. 6, top and bottom left), whereas the anomalous stratospheric radiative heating drives a westerly acceleration in the stratosphere but an easterly acceleration in the troposphere (Fig. 6, left). Hence at tropospheric levels, the balanced response to negative anomalous stratospheric heating opposes the westerly forcing due to frictional damping in the boundary layer. The combined simulated tendencies bear a strong resemblance to the observed tendencies at both stratospheric and tropospheric levels (Fig. 6, right panels; Fig. 2, bottom panels).

Figure 7 summarizes the time-integrated responses of

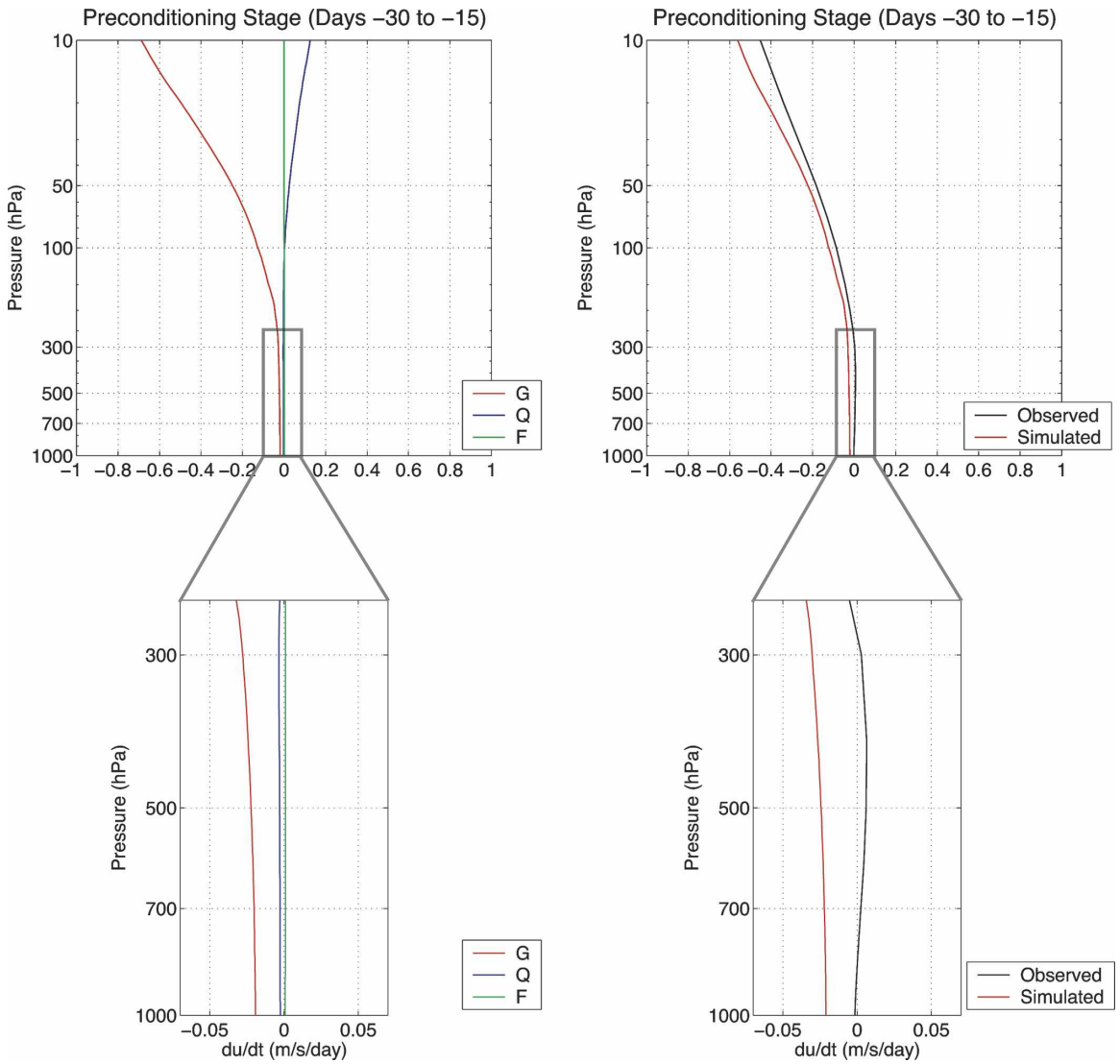

FIG. 4. (top) Zonal-mean zonal wind tendencies averaged over 55°–75°N and over the preconditioning stage (days −30 to −15). (left) Vertical profiles of the model derived zonal-mean zonal wind tendencies. Red lines denote the response to stratospheric wave driving (G), blue lines the response to stratospheric radiative heating (Q), and green lines the response to friction (F). (right) The sum of the model-derived tendencies from the (left) (red) and the corresponding observed tendencies (black). (bottom) As in the (top), but for results highlighted at tropospheric levels.

the tendencies in the near-surface zonal-mean zonal flow during the growth and maintenance stages; that is, those periods coinciding with the observed tropospheric response. The top panel shows the integrated responses to the three forcings separately; the bottom panel shows the combined simulated response alongside the corresponding observed zonal-mean zonal wind anomalies. The figure highlights the two key findings reported in this section: 1) the balanced response to anomalous stratospheric wave drag is quantitatively similar to the observed tropospheric response during the growth stage (top and bottom panels); and 2) the balanced response to anomalous stratospheric radiative heating acts to oppose the effects of frictional dissipation in the boundary layer and hence increases the persistence of the tropospheric anomalies (top panel).

4. Discussion

The results in the previous section reveal that the balanced response to stratospheric wave drag and radiative heating anomalies is sufficiently large to account for the amplitude and persistence of the observed tropospheric response to stratospheric variability. As such,

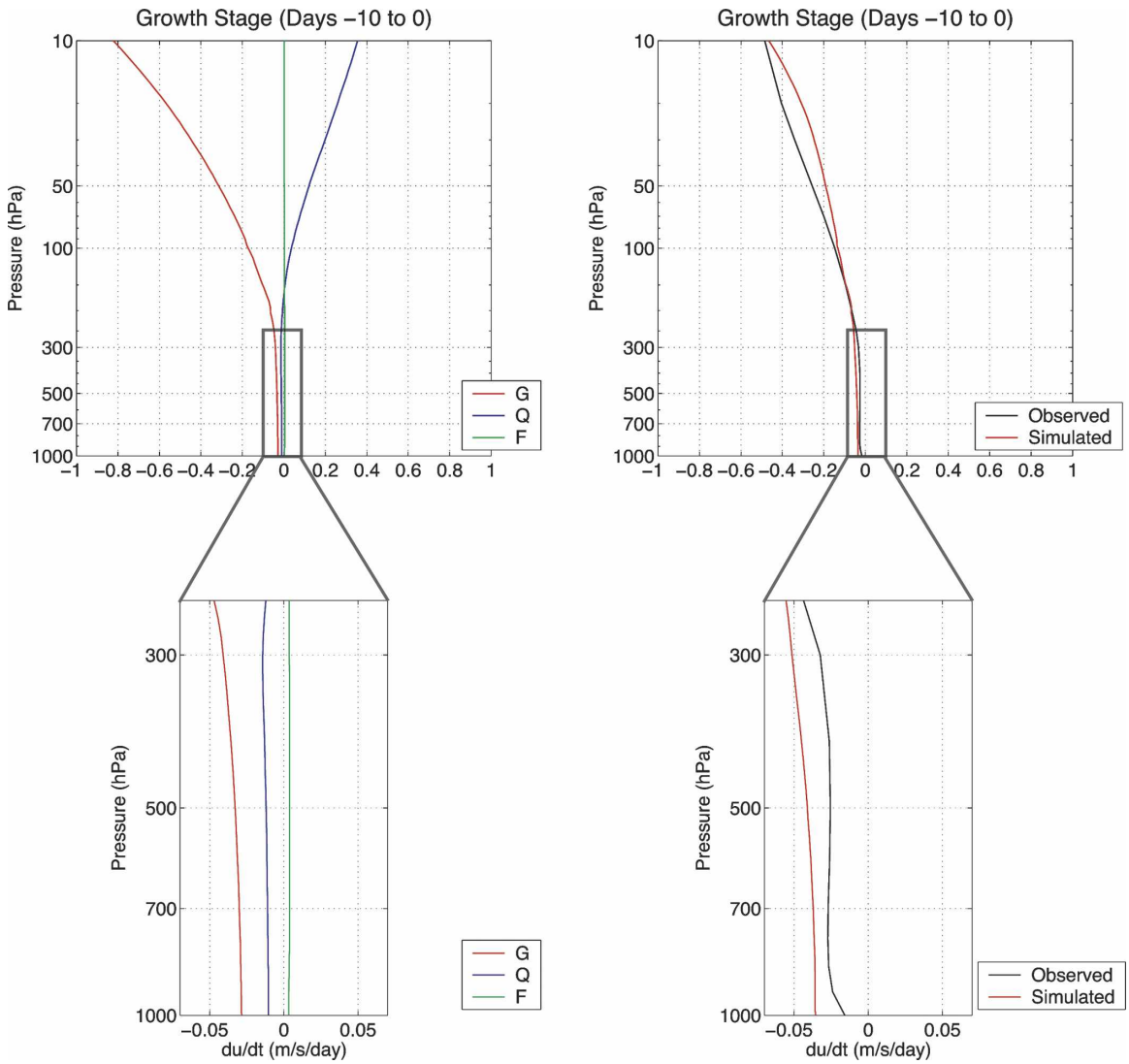

FIG. 5. As in Fig. 4, but for results averaged over the growth stage (days −10 to 0).

the results suggest that amplification due to internal tropospheric feedbacks is not required to explain the amplitude of the tropospheric anomalies. However, while our approach has implications for the amplitude of the tropospheric response, it does not necessarily reveal the mechanisms that give rise to the tropospheric response in the first place. The limitations of our approach are discussed below.

As a starting point for the discussion, consider the hypothetical distributions of the EP flux and its divergence shown in Fig. 8. Both distributions are associated with identical stratospheric wave driving but very different wave flux distributions and hence very different forcing of the tropospheric circulation. In Fig. 8a, the wave flux anomalies are dominated by vertical propagation across the high-latitude tropopause. In this case, the source of the anomalous wave activity lies directly underneath the region of stratospheric EP flux convergence and the vertically integrated EP flux divergence is zero at all latitudes. Thus the tropospheric circulation can be viewed as shielded from the impact of the anomalous stratospheric wave drag since the induced circulation will largely close within the stratosphere and upper troposphere.

In contrast, in Fig. 8b the wave flux anomalies are characterized by vertical propagation across the high-latitude tropopause and poleward wave propagation in the upper troposphere at middle latitudes. Since the source of the anomalous wave activity is shifted equatorward of the region of stratospheric wave drag, the vertically integrated EP flux divergence is positive at subtropical latitudes and negative at subpolar latitudes.

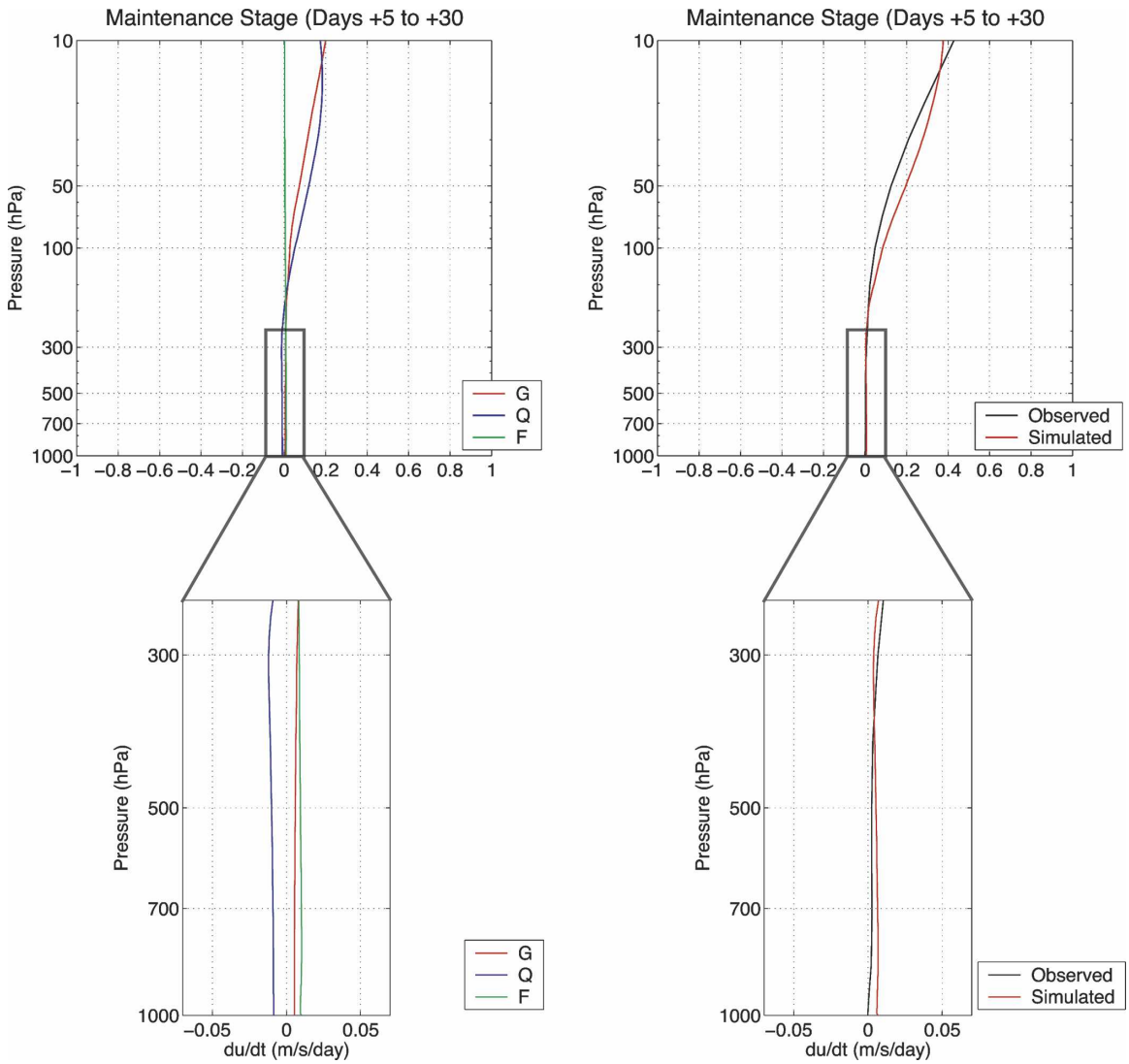

FIG. 6. As in Fig. 4, but for results averaged over the maintenance stage (days +5 to +30).

In this case, the anomalous wave flux into the stratosphere is quantitatively similar to the anomalous poleward wave flux in the middle latitude troposphere.

From the above thought experiment, it follows that the surface flow responds not to the changes in vertical wave propagation into the stratosphere, but rather to the vertically integrated changes in the meridional flux of wave activity and hence of eddy momentum (this is strictly true at the steady-state limit). The importance of the vertically integrated eddy momentum flux in driving the surface flow is discussed in Held and Andrews (1983). It is also highlighted in Shepherd and Shaw (2004), who argue that true downward influence arises only through changes in the meridional flux of wave activity or wave reflection.

A similar line of reasoning can be used to interpret the relationship between the meridional distributions of the EP flux and the observed changes in the tropospheric flow during the preconditioning, growth, and maintenance stages (Fig. 9). During the preconditioning stage (top), the anomalous wave fluxes are predominantly upward, and the tropospheric flow does not exhibit noticeable changes despite considerable anomalous stratospheric wave drag at this time. During the growth stage (middle), the anomalous wave fluxes have a more substantial meridional component near the midlatitude tropopause. At this time, in the upper troposphere near ~60°N the anomalous meridional convergence of the EP flux (blue contours) acts to oppose the anomalous vertical divergence of the EP flux (red con-

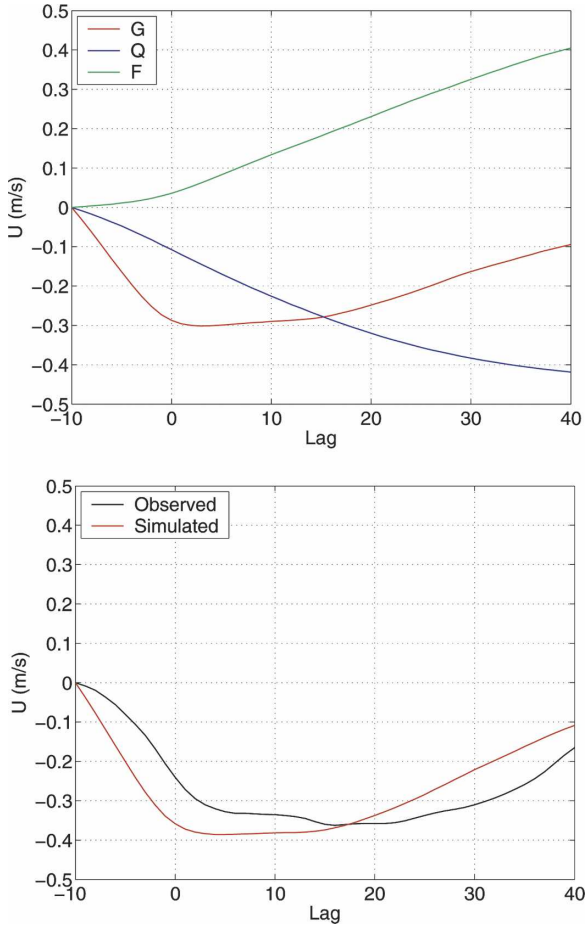

FIG. 7. (top) The time-integrated response of the zonal-mean zonal wind averaged over 55°–75°N at 925 hPa to G (red), F (green), and Q (blue). (bottom) The total simulated response (red) and the corresponding observed zonal-mean zonal wind anomalies (black). All wind anomalies are shown with respect to their values at day −10.

Profile a)
Vertical wave propagation into the stratosphere.
No change in the vertically integrated EP-flux divergence.

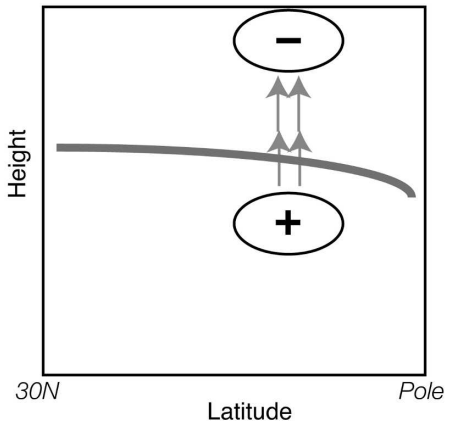

Profile b)
Vertical wave propagation into the stratosphere
is accompanied by meridional wave propagation
in the upper troposphere.

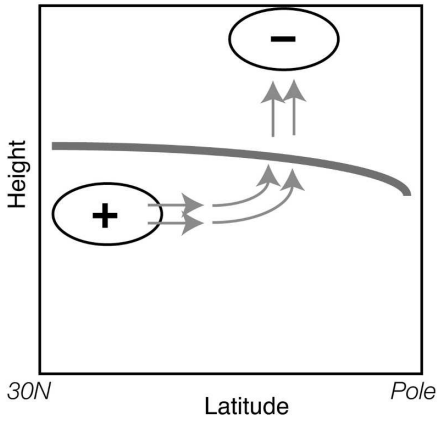

FIG. 8. Schematic profiles of the EP flux (gray arrows) and its divergence (plus symbol) and convergence (minus symbol). The horizontal sloping gray line denotes the tropopause. See text for details.

tours), and the tropospheric flow accelerates easterly in a manner consistent with the balanced response to the overlying stratospheric wave drag. During the maintenance stage (bottom), there is substantial eddy momentum forcing in the upper troposphere but only weak net wave forcing at stratospheric levels.

Thus the approach used in this study reveals that the amplitude of the changes in the tropospheric flow is closely related to the amplitude of the anomalous stratospheric wave drag. However, the approach does not necessarily reveal the mechanisms that drive the tropospheric anomalies, since the calculations do not consider the pattern of compensating wave forcing at tropospheric levels. It is unclear why the amplitude of the tropospheric response should be quantitatively similar to the effect of the stratospheric wave forcing, particularly since the tropospheric and stratospheric responses are driven by very different wave types: the former is linked to anomalous meridional propagation by synoptic-scale waves; the latter to anomalous vertical propagation by waves with zonal wavenumbers 1 and 2 (Limpasuvan et al. 2004). Nevertheless, it is worth noting that the observed changes in tropospheric momentum fluxes are consistent with the simulated impact of anomalous barotropic shear on the flux of momentum by decaying baroclinic waves (Thorncroft et al. 1993; Hartmann and Zuercher 1998).

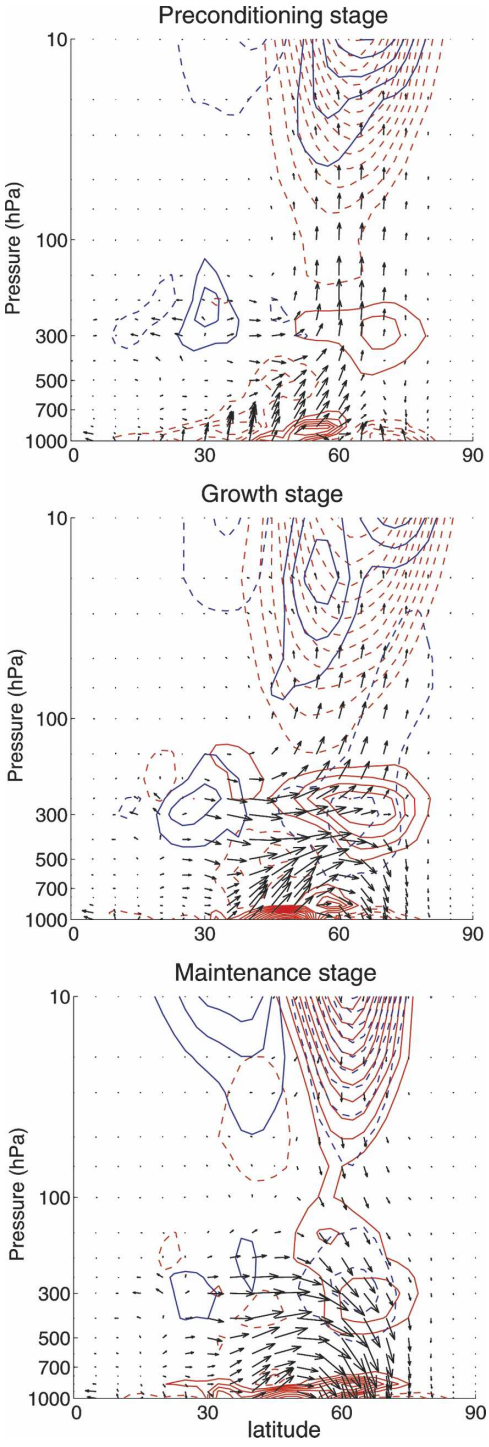

FIG. 9. The EP flux anomalies (vectors) and the horizontal (blue contours) and vertical (red contours) components of the corresponding divergences regressed onto standardized and inverted JFM values of the NAM_{10} index time series. Results are shown for the (top) preconditioning, (middle) growth, and (bottom) maintenance stages. The longest vector is $\sim 1 \times 10^7$ J m^{-2}. Contour interval is 0.1 m s^{-1} day^{-1}.

5. Concluding remarks

The results in this study highlight the following previously overlooked aspects of stratosphere/troposphere dynamical coupling:

1) The amplitude of the observed tropospheric response to stratospheric variability is quantitatively similar to the balanced response to anomalous wave drag at stratospheric levels.
2) Anomalous radiative heating at stratospheric levels contributes to the persistence of the tropospheric response to stratospheric variability.

The first result demonstrates that amplification due to internal tropospheric feedbacks is not required to explain the amplitude of the tropospheric anomalies, but it does not necessarily reveal the mechanisms that drive the tropospheric response in the first place. The second result provides a conceptually simple but previously overlooked mechanism whereby stratospheric variability imparts persistence to the tropospheric circulation.

The above conclusions contradict previous studies that suggest internal tropospheric dynamics must somehow amplify the observed tropospheric response for at least two reasons:

1) The time scale of the response in Kushner and Polvani (2004) is roughly 10 times longer than the time scale of the observed relationships. At such long time scales, the surface response to stratospheric heating is substantially less than that simulated in section 3.
2) Previous studies are based on analyses of the tropospheric component of the annular mode (e.g., Song and Robinson 2004), whereas as noted in section 2 the tropospheric response to stratospheric variability is best estimated from analyses of the stratospheric component of the annular mode. The impact of the choice of the level used as a basis of the regressions is further exemplified in Fig. 10. Regressions based on variations in the NAM at stratospheric levels are associated with minimum EP flux divergence anomalies at 50 hPa of -0.4 m s^{-1} day^{-1} and minimum zonal-mean zonal wind tendencies at 925 hPa of -0.04 m s^{-1} day^{-1}, a ratio of about 10:1. In contrast, regressions based on variations in the NAM at lower tropospheric levels yield analogous ratios of only about 1:1.

The conclusions in this study suggest future research on stratosphere/troposphere dynamical coupling focus not on the feedbacks required to amplify the tropospheric response but on the following two questions:

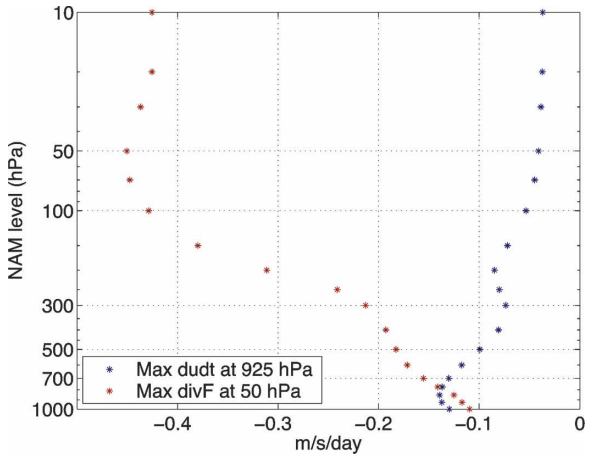

FIG. 10. Regressions onto standardized and inverted JFM values of the NAM index time series at different levels. Blue represents minimum anomalies of the EP flux divergence at 50 hPa averaged over 55°–75°N. Red represents minimum anomalous tendencies in the zonal-mean zonal wind at 925 hPa averaged over 55°–75°N. Minimum anomalies are drawn from regressions for all lags −41 to +41 days. The ordinate axis corresponds to the base level used to define the NAM index. For example, the values at 10 hPa correspond to the minimum values of the EP flux divergence at 50 hPa and the minimum tendencies in the zonal-mean zonal wind at 925 hPa observed in Fig. 1.

1) What processes give rise to the vertical flux of wave activity across the tropopause? This question is relevant not only for predicting the onset of the stratospheric wave event, but also the rapid change in sign of the stratospheric wave drag at the end of the growth stage.
2) What processes give rise to the change in the meridional flux of wave activity at tropospheric levels? This question is key for understanding the attenuation of the shielding of the high-latitude troposphere and the meridional redistribution of momentum within the troposphere.

Acknowledgments. D. W. J. Thompson and J. C. Furtado are supported by the National Science Foundation Climate Dynamics program, and T. G. Shepherd is supported by the Natural Sciences and Engineering Research Council of Canada and the Canadian Foundation for Climate and Atmospheric Sciences. The authors thank W. Robinson for his characteristically insightful review of the manuscript, R. Black for useful discussions, and an anonymous reviewer for helpful comments.

REFERENCES

Ambaum, M. H. P., and B. J. Hoskins, 2002: The NAO troposphere–stratosphere connection. *J. Climate,* **15,** 1969–1978.

Andrews, D. G., J. R. Holton, and C. B. Leovy, 1987: *Middle Atmosphere Dynamics.* Academic Press, 489 pp.

Baldwin, M. P., and T. J. Dunkerton, 1999: Propagation of the Arctic Oscillation from the stratosphere to the troposphere. *J. Geophys. Res.,* **104,** 30 937–30 946.

——, and ——, 2001: Stratospheric harbingers of anomalous weather regimes. *Science,* **294,** 581–584.

——, X. Cheng, and T. J. Dunkerton, 1994: Observed correlations between winter-mean tropospheric and stratospheric circulation anomalies. *Geophys. Res. Lett.,* **21,** 1141–1144.

Black, R. X., 2002: Stratospheric forcing of surface climate in the Arctic Oscillation. *J. Climate,* **15,** 268–277.

Boville, B. A., 1984: The influence of the polar night jet on the tropospheric circulation in a GCM. *J. Atmos. Sci.,* **41,** 1132–1142.

Bretherton, C. S., M. Widmann, V. P. Dymnikov, J. M. Wallace, and I. Bladé, 1999: The effective number of spatial degrees of freedom of a time-varying field. *J. Climate,* **12,** 1990–2009.

Chen, P., and W. A. Robinson, 1992: Propagation of planetary waves between the troposphere and stratosphere. *J. Atmos. Sci.,* **49,** 2533–2545.

Cheng, X., 1993: Linear and nonlinear aspects of the Northern Hemisphere wintertime variability in the 500-hPa height field. Ph.D. dissertation, University of Washington, 180 pp.

COESA, 1976: *U.S. Standard Atmosphere.* U.S. Government Printing Office, 227 pp.

Dickinson, R. E., 1968: On the excitation and propagation of zonal winds in an atmosphere with Newtonian cooling. *J. Atmos. Sci.,* **25,** 269–279.

Edmon, H. J., Jr., B. J. Hoskins, and M. E. McIntyre, 1980: Eliassen–Palm cross sections for the troposphere. *J. Atmos. Sci.,* **37,** 2600–2615.

Eliassen, A., 1951: Slow thermally or frictionally controlled meridional circulation in a circular vortex. *Astrophys. Norv.,* **5,** 19–60.

Feldstein, S. B., 2000: The timescale, power spectra, and climate noise properties of teleconnection patterns. *J. Climate,* **13,** 4430–4440.

Hartley, D. E., J. Villarin, R. X. Black, and C. A. Davis, 1998: A new perspective on the dynamical link between the stratosphere and troposphere. *Nature,* **391,** 471–474.

Hartmann, D. L., and P. Zuercher, 1998: Response of baroclinic life cycles to barotropic shear. *J. Atmos. Sci.,* **55,** 297–313.

Haynes, P. H., and T. G. Shepherd, 1989: The importance of surface pressure changes in the response of the atmosphere to zonally-symmetric thermal and mechanical forcing. *Quart. J. Roy. Meteor. Soc.,* **115,** 1181–1208.

——, M. E. McIntyre, T. G. Shepherd, C. J. Marks, and K. P. Shine, 1991: On the "downward control" of extratropical diabatic circulations by eddy-induced mean zonal forces. *J. Atmos. Sci.,* **48,** 651–680.

Held, I. M., and D. G. Andrews, 1983: On the direction of the eddy momentum flux in baroclinic instability. *J. Atmos. Sci.,* **40,** 2220–2231.

Kitoh, A., H. Koide, K. Kodera, S. Yukimoto, and A. Nodo, 1996: Interannual variability in the stratospheric-tropospheric circulation in a coupled ocean-atmosphere GCM. *Geophys. Res. Lett.,* **23,** 543–546.

Kushner, P. J., and L. M. Polvani, 2004: Stratosphere–troposphere coupling in a relatively simple AGCM: The role of eddies. *J. Climate,* **17,** 629–639.

Limpasuvan, V., D. W. J. Thompson, and D. L. Hartmann, 2004:

The life cycle of the Northern Hemisphere sudden stratospheric warmings. *J. Climate,* **17,** 2584–2596.

Norton, W. A., 2003: Sensitivity of Northern Hemisphere surface climate to simulation of the stratospheric polar vortex. *Geophys. Res. Lett.,* **30,** 1627, doi:10.1029/2003GL016958.

Perlwitz, J., and H.-F. Graf, 1995: The statistical connection between tropospheric and stratospheric circulation of the Northern Hemisphere in winter. *J. Climate,* **8,** 2281–2295.

——, and N. Harnik, 2003: Observational evidence of a stratospheric influence on the troposphere by planetary wave reflection. *J. Climate,* **16,** 3011–3026.

Polvani, L. M., and P. J. Kushner, 2002: Tropospheric response to stratospheric perturbations in a relatively simple general circulation model. *Geophys. Res. Lett.,* **29,** 1114, doi:10.1029/2001GL014284.

Reichler, T., P. J. Kushner, and L. M. Polvani, 2005: The coupled stratosphere–troposphere response to impulsive forcing from the troposphere. *J. Atmos. Sci.,* **62,** 3337–3352.

Shepherd, T. G., and T. A. Shaw, 2004: The angular momentum constraint on climate sensitivity and downward influence in the middle atmosphere. *J. Atmos. Sci.,* **61,** 2899–2908.

Shindell, D. T., R. L. Miller, G. Schmidt, and L. Pandolfo, 1999: Simulation of recent northern winter climate trends by greenhouse gas forcing. *Nature,* **399,** 452–455.

Simmons, A. J., and J. K. Gibson, 2000: The ERA-40 Project Plan. ERA-40 Project Report Series 1, 61 pp.

Song, Y., and W. A. Robinson, 2004: Dynamical mechanisms for stratospheric influences on the troposphere. *J. Atmos. Sci.,* **61,** 1711–1725.

Taguchi, M., 2003: Tropospheric response to stratospheric degradation in a simple global circulation model. *J. Atmos. Sci.,* **60,** 1835–1846.

Thompson, D. W. J., and J. M. Wallace, 1998: The Arctic Oscillation signature in the wintertime geopotential height and temperature fields. *Geophys. Res. Lett.,* **25,** 1297–1300.

——, and ——, 2000: Annular modes in the extratropical circulation. Part I: Month-to-month variability. *J. Climate,* **13,** 1000–1016.

Thorncroft, C. D., B. J. Hoskins, and M. E. McIntyre, 1993: Two paradigms of baroclinic life-cycle behaviour. *Quart. J. Roy. Meteor. Soc.,* **119,** 17–55.